6566 *Inorg. Chem.* **2009**, *48*, 6566–6572
DOI: 10.1021/ic9005482

Inorganic Chemistry
Article

Structure Determination of $La_{18}W_{10}O_{57}$

Marie-Hélène Chambrier,*,† Armel Le Bail,† Stéphanie Kodjikian,† Emmanuelle Suard,‡ and François Goutenoire†

†*Laboratoire des Oxydes et Fluorures, UMR-CNRS 6010, Université du Maine, 72085 Le Mans Cedex 9, France, and* ‡*Institut Laue Langevin, Avenue des Martyrs, B.P. 156, 38042 Grenoble Cedex 9, France*

Received March 20, 2009

We report the synthesis, structure determination, and structure analysis of $La_{18}W_{10}O_{57}$, which presents 52.65 WO_3 mol % in the binary system $La_2O_3-WO_3$ in place of the previous reported compound: $La_{14}W_8O_{45}$, 53.3 WO_3 mol %. The structure has been determined from synchrotron and laboratory X-ray, neutron, and electron diffraction data. This tungstate crystallizes in the non-centrosymmetric hexagonal space group (no. 190) $P\bar{6}2c$, with $Z = 2$, $a = 9.0448(1)$ Å, $c = 32.6846(3)$ Å, and a measured density of 7.28(3) $g \cdot cm^{-3}$. The structure consists of [WO_6] octahedra, isolated or sometimes sharing a face, and unusual tungsten [WO_6] trigonal prisms. This compound presents a subcell $c' = c/6 = 5.45$ Å. Polytypism has been observed concerning this compound. Transmission electronic microscopy, ionic conductivity, and thermal expansion have been explored.

Introduction

Oxides in the family $Ln_2O_3-MO_3$ (M = Mo and W) have been studied in the past for their refractory and nuclear materials, laser host, and ferroelectric applications. More recently, oxide ionic conduction has been discovered in the molybdate and the tungstate high-temperature form of $La_2M_2O_9$ (M = Mo and W).[1,2] Maybe associated with this last physical property, the low thermal conductivity at high temperature behavior has been pointed out for $La_2Mo_2O_9$.[3]

As for the $La_2O_3-MoO_3$ phase diagram,[4] many reported compositions have not been correctly characterized in the $La_2O_3-WO_3$ system. This last phase diagram has been reported many times.[5] Most of the time, around the composition 50 WO_3 mol % only La_2WO_6 is reported with a solid solution. Yoshimura et al.[5] proposed the composition $La_{14}W_8O_{45}$, and Yanovskii et al.[5] mentioned a solid solution from 50 to ~55.5 in WO_3 mol % corresponding to the formula $La_2W_{1+x}O_{6+3x}$ with a maximum value of x equal to 0.25, leading to the formula $La_2W_{1.25}O_{6.75}$.

We now report the synthesis, structure determination, and structure analysis of $La_{18}W_{10}O_{57}$, which presents 52.65 WO_3 mol % in place of $La_{14}W_8O_{45}$ 53.3 WO_3 mol %.

Experimental Section

The synchrotron diffraction pattern was collected on a Debye–Scherrer diffractometer, BM01A, instrument at ESRF, Grenoble. Data collection was performed on a 0.3 mm capillary at 0.60044 Å wavelength from 1° to 45° with an increment step of 0.003° for a total counting time of ~3 h.

High-temperature X-ray diffraction patterns were collected on a Bragg–Brentano diffractometer (MPD-PRO Panalytical) with copper radiation equipped with an X'celerator linear detector (Ni Filter) and an Anton Paar HTK12 furnace. The high-temperature X-ray diffraction patterns were collected during one night, from [5°–70°, 2θ], at 30, 200, 400, 800, and 1000 °C. Neutron diffraction data were collected on the powder diffractometer, D2B (instrument at ILL, Grenoble). Data collections were performed at ~1.59398(4) Å wavelength on ~15 g of compound at room temperature. For the pattern the increment step was 0.05° (2θ), the interval of data collection ranged from 0° to 162°, and the total counting time was ~2 h with a high flux and medium-resolution configuration.

The electron diffraction study was performed on a 200 kV side entry JEOL2010 transmission electron microscope with a double-tilt specimen holder operating at room temperature. The sample was prepared by grinding a small amount of powder in an agate mortar and pestle under dry 1-butanol to produce a suspension. A drop of the suspension was deposited on a holey carbon film supported by a 1000 mesh copper grid and dried.

The density measurement was performed on an ACCUPIC 1330 gas picnometer (Micromeritics) with helium as gas using

*To whom correspondence should be addressed. E-mail: marie-helene.chambrier.etu@univ-lemans.fr.

(1) Lacorre, P.; Goutenoire, F.; Bohnke, O.; Retoux, R.; Laligant, Y. *Nature* **2000**, *404*, 856–858.
(2) Marrero-Lopez, D.; J. Pena-Martínez, J.; Ruiz-Morales, J. C.; Nunez, P. *J. Solid State Chem.* **2008**, *181*, 253–262.
(3) Winter, M. R.; Clarke, D. R. *J. Am. Ceram. Soc.* **2007**, *90*(2), 533–570.
(4) Fournier, J. P.; Kohlmuller, R. *Bull. Soc. Chim. Fr.* **1970**, *12*, 4277–4279.
(5) Acer-Nist, phase Equilibria Diagram, Fig. 06484: Rode, E.; Ya, M.; Balagina, G.; Ivanova, M. M.; Karpov, V. N. *Zh. Neorg. Khim.* **1968**, *13* (5), 1451–1456; *Russ. J. Inorg. Chem. (Engl. Transl.)* **1968**, *13* (5), 762–765. Fig. 93-047: Yoshimura, M.; Rouanet, A. *Mater. Res. Bull.* **1976**, *11* (2), 151–158. Fig. 04424: Ivanova, M. M.; Balagina, G. M.; Rode, E. Ya. *Izv. Akad. Nauk SSSR, Neorg. Mater.* **1970**, *6* (5), 914–919; *Inorg. Mater. (Engl. Transl.)* **1970**, *6* (5) 803–805. Fig. 06485: Casteels, F. G.; Brabers, M. J.; DePaus, R. *Rev. Int. Hautes Temp. Refract.* **1980**, *16* (4), 424–436. Fig. 09939: Yanovskii, V. K.; Voronkova, V. I. *Izv. Akad. Nauk SSSR, Neorg. Mater.*, **1983**, *19* (3), 416–421; *Inorg. Mater. (Engl. Transl.)* **1983**, *19* (3), 375–379.

 Published on Web 06/22/2009

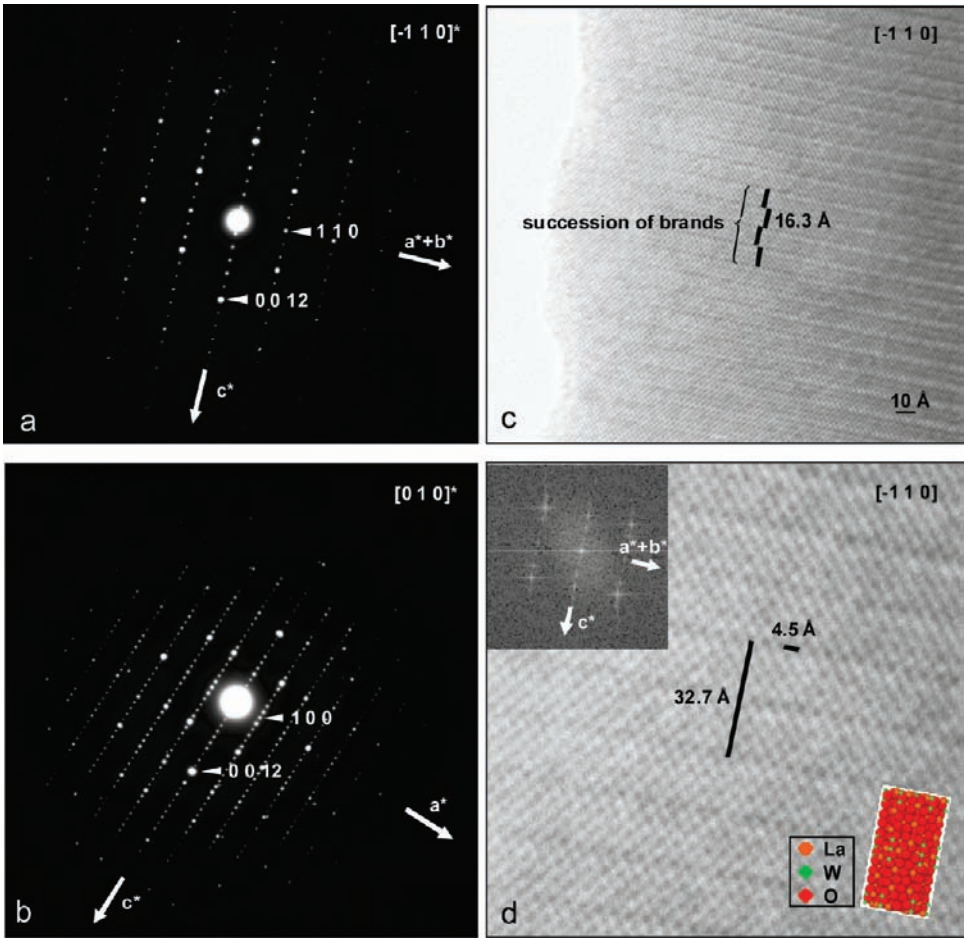

Figure 1. [−1 1 0]* (a) and [0 1 0]* (b) SAED patterns for $La_{18}W_{10}O_{57}$. [−1 1 0] HREM image (c) of $La_{18}W_{10}O_{57}$ and zoom (d). A succession of brands is evidenced. The Fourier transform is shown in the inset. A projection of the structure along [−1 1 0] is superimposed with the experimental image.

approximately 2 g of sample. The temperature of measurement was 24 ± 1 °C.

The ionic conductivity measurement of this compound was performed by complex impedance spectroscopy in the 10 MHz to 1 Hz frequency range with an applied voltage of 100 mV using a Solartron SI 1260 impedance gainphase analyzer with Smart[6] impedance software for data acquisition. The measurements were performed on pellets of 5 mm diameter and 4 mm thickness, with platinum deposited on both faces as electrodes. Impedance data were obtained in the 700−100 °C temperature range under N_2. The sample was allowed to equilibrate for 30 min at each temperature prior to data acquisition, in order to be in thermodynamical equilibrium.

Results and Discussion

Synthesis. The compound was prepared with La_2O_3 and WO_3 as starting oxides. Lanthanum oxide powder was dried and decarbonated at 1000 °C overnight prior to use. The oxides were weighed in stoichiometric proportions with a 7:8 molar ratio of La_2O_3 and WO_3 and ground together in an agate mortar. The prepared composition was heated to 1400 °C for one night in an alumina crucible; no particular condition was used in order to cool the samples. For the X-ray measurement a small amount (∼0.5 g) of the compound with final formula was synthesized. For the neutron data a larger amount of compound was prepared (∼15 g) with the $La_{14}W_8O_{45}$ composition. The final compound was white.

The X-ray diffraction pattern was rather similar to the compound $La_{14}W_8O_{45}$ previously studied by Yoshimura[5] with the JCPDF reference 00-032-0502. The difference in the formulation between $La_{14}W_8O_{45}$ and $La_{18}W_{10}O_{57}$ is rather small. The composition of $La_{14}W_8O_{45}$ leads to the WO_3 composition of $8/(7 + 8) = 53.3\%$, whereas $La_{18}W_{10}O_{57}$ leads to the WO_3 composition of $10/(9 + 10) = 52.6\%$ in the phase diagram $La_2O_3-WO_3$. We were unable to see such a difference during the synthesis. A larger amount of WO_3 leads to $La_2W_2O_9$[7] as an impurity. On the contrary, a smaller amount of WO_3 leads to La_2WO_6[8] as an impurity. The two previous compounds have respectively 66.6% and 50% WO_3.

Electron Diffraction (ED) and High-Resolution Electron Microscopy (HREM). Selected area electron diffraction was performed. Thin spots were observed indicating that the compound was well crystallized (Figure 1a). ED patterns were indexed on a hexagonal lattice with cell parameters $a \approx 9.0$ Å, $c \approx 32.7$ Å. Tilting crystals along different reciprocal lattice directions revealed the existence condition $00l$, $l = 2n$ (Figure 1a), which was assigned

(6) Solartron Materials Research and test software 2004.

(7) Laligant, Y.; Le Bail, A.; Goutenoire, F. *J. Solid State Chem.* **2001**, *159*, 223–227.

(8) Chambrier, M.-H.; Kodjikian, S.; Ibberson, R. M.; Goutenoire, F. *J. Solid State Chem.* **2008**, *182*, 209–214.

to a primitive lattice with conditions *hh*-2*hl* ($l = 2n$) and 000*l* ($l = 2n$), leading to the following space groups: $P6_3/mmc$ (no. 194), $P\bar{6}2c$ (no. 190, non-centrosymmetric), and $P6_3mc$ (no. 186, non-centrosymmetric). However, weak reflections can appear at the extinct positions 00*l* with *l* odd, due to double diffraction, as on the ED pattern corresponding to the [010] zone axis (Figure 1b).

In addition, we note that strong and weak spots were simultaneously present; considering intense spots only, a subcell with the new parameter $c' = c/6 \approx 5.5$ Å was obtained.

A HREM study along the [−110] zone axis was performed, exhibiting a regular succession of bands along the *c* axis (Figure 1c). Unfortunately, no image could be calculated with the EMS computer program[9] because of the large number of atoms in the cell. However, considering both the arrangement of the W atoms in the structure and the distance between two brands along [001], we superimposed the projection of the structure with the experimental image (Figure 1d). No default was evidenced, which was in good agreement with the well-defined spots mentioned previously.

Crystal Structure Determination. The cell is confirmed by a satisfying whole powder pattern fit (WPPF) by using the Le Bail method[10] through the Fullprof software.[11] The extracted intensities from the synchrotron powder pattern were then used for attempting the structure solution by direct space methods as embedded in the ESPOIR software,[12] searching for the heavy W and La independent atoms by a Monte Carlo process. Nothing better than $R_p > 35\%$ could be obtained during various tests in the $P6_3/mmc$ or $P6_3mc$ space groups. Direct or Patterson methods failed as well to provide a satisfying starting model. Then the search for a solution was made in the *c*/6 subcell, in spite of the fact that very intense reflections had to be excluded (scaling the most intense 206 at $I = 100$, the 207 is at $I = 13$, the 217 is at $I = 14$). Trying various space groups without extinction, a promising model leading to R_p=22% on 220 remaining peaks was finally obtained from the ESPOIR software in the $P\bar{6}2m$ space group, corresponding to a La/W = 2 ratio (La_2WO_6 formula). No extension of that model in the large cell could be obtained in the $P6_3/mmc$ or $P6_3mc$ space groups. Then the other space groups compatible with the *hh*-2*hl*, $l = 2n$, reflection condition were examined ($P\bar{6}2c$, $P\bar{3}1c$, $P31c$). The small initial (Table 1) model could be extended in the large cell by using the acentric space groups, for instance with 4 La and 5 W independent atom sites in the general or special positions of $P\bar{6}2c$. Using that estimation of the number of independent sites, ESPOIR provided new starting coordinates for the La and W atoms in the large cell, decreasing R_p to a satisfying 23%. Introducing these atomic coordinates into a Rietveld[13] refinement led then to R_B = 19.7 and R_F = 11.1% when the thermal parameters were refined (most having negative values because of the absence of absorption correction at this stage). From a Fourier difference map, an additional W atom site was detected as well as all the oxygen atoms in 10 independent sites. Refinement and structure analysis suggested that this new W site had to be half-occupied, leading to the $La_{18}W_{10}O_{57}$ formula with $Z = 2$. Some of the W atoms were found in octahedral coordination, but the majority of them are in an unusual trigonal prismatic coordination. We then tried to confirm that by a new search for the oxygen atom position from the neutron data by using the ESPOIR software, fixing the La and W atoms to the positions obtained from the synchrotron data refinements. The same model was built up by ESPOIR from the neutron data. This unusual trigonal prismatic coordination was previously observed for the WO_6 group in the X-ray studies of $Pr_3WO_6Cl_3$[14] and $La_3WO_6Cl_3$,[15] the latter structure being then confirmed from neutron powder diffraction data.[16] Indeed,

Table 1. Initial Model for $La_{18}W_{10}O_{57}$ in the *c*/6 Subcell in the $P\bar{6}2m$ Space Group, Compared to the W and La Positions in the $La_3WO_6Cl_3$ Structure Described in the $P6_3/m$ Space Group

atom	Wyckoff	*x*	*y*	*z*
		c/6 Subcell of $La_{18}W_{10}O_{57}$		
W1	1a	0	0	0
W2	2d	1/3	2/3	1/2
La1	3f	0.429	0	0
La2	3g	0.743	0	1/2
		$La_3WO_6Cl_3$		
W	2c	1/3	2/3	1/4
La	6h	0.0906	0.6865	3/4

Table 2. Crystallographic Parameters of $La_{18}W_{10}O_{57}$ Obtained from Mixed Refinement[a]

atom	position	*x*	*y*	*z*	B_{iso} (Å)
La1	12i	0.6154(7)	0.0393(6)	0.5837(2)	1.5(1)
La2	12i	0.2766(5)	0.0355(4)	0.3316(1)	0.7(1)
La3	6h	0.3711(8)	0.4298(9)	1/4	0.9(1)
La4	6g	0.2565(8)	0	0	0.9(2)
W1	4e	0	0	0.5850(2)	0.9(1)
W2	4f	1/3	2/3	0.3332(2)	0.8(1)
W3	4f	1/3	2/3	0.0032(2)	0.8(1)
W4	4f	1/3	2/3	0.6365(2)	2.4(1)
W5	2b	0	0	1/4	0.6(2)
W6[b]	4f	1/3	2/3	0.2811(3)	0.9(2)
O1	12i	−0.169(2)	−0.016(2)	0.2126(4)	1.1(3)
O2	12i	−0.024(2)	−0.175(2)	0.6214(4)	0.6(2)
O3	12i	0.695(2)	0.512(2)	0.7039(3)	0.8(2)
O4	12i	0.518(2)	0.708(2)	0.0456(3)	0.4(2)
O5	12i	0.675(1)	0.502(2)	0.6298(3)	0.9(2)
O6	12i	0.155(2)	0.179(2)	0.5463(4)	1.3(2)
O7	12i	0.472(1)	0.185(1)	0.3919(3)	0.7(2)
O8	12i	0.140(2)	0.598(2)	−0.0226(4)	2.7(3)
O9	6 h	0.469(2)	0.179(3)	1/4	1.9(3)
O10	12i	0.513(2)	0.366(2)	0.3241(1)	1.8(2)

[a] Synchrotron: 1086 reflections, R_{Bragg} = 6.55%, R_{wp} = 18.1%. Neutron: 940 reflections R_{Bragg} = 6.48%, R_{wp} = 15.1%. Space group $P\bar{6}2c$ (no. 190), a = 9.0448(1) Å, c = 32.6846(3) Å, Z = 2, calculated density = 7.52 g·cm^{-3}, measured density = 7.28(3) g·cm^{-3}. [b] Half-occupied site.

(9) Stadelmann, P. *Ultramicroscopy* **1981**, *14*, 149.
(10) Le Bail, A.; Duroy, H.; Fourquet, J. L. *Mater. Res. Bull.* **1988**, *23*, 447–452.
(11) Rodriguez-Carvajal, J., *Abstracts of the Satellite Meeting on Powder Diffraction of the XV Congress of the IUCr*; Toulouse, France, 1990; p 127.
(12) Le Bail A. *ESPOIR*: A program for solving structures by Monte Carlo from powder diffraction data. *Mater. Sci. Forum*, **2001**, *378*−*381*, 65−70.
(13) Rietveld, H. M. *J. Appl. Crystallogr.* **1969**, *2*, 65–71.
(14) Polyanskaya, T. M. *Dokl. Akad. Nauk SSR* **1969**, *187*, 1043.
(15) Brixner, L. H.; Chen, H. Y.; Foris, C. M. *J. Solid State Chem.* **1982**, *44*, 99–107.
(16) Parise, J. B.; Brixner, L. H. *Acta Crystallogr.* **1983**, *C39*, 1326–1328.

Table 3. Selected Bond Distances (Å) for $La_{18}W_{10}O_{57}$

La1−O2	2.511(1)	La2−O1	2.55(1)	La3−O1 × 2	2.51(1)	La4−O4 × 2	2.42(1)
La1−O4	2.42(1)	La2−O1	2.48(1)	La3−O3 × 2	2.57(1)	La4−O6 × 2	2.39(2)
La1−O4	2.554(2)	La2−O2	2.583(2)	La3−O3 × 2	2.517(2)	La4−O6 × 2	2.69(2)
La1−O5	2.48(2)	La2−O2	2.56(1)	La3−O9	2.817(3)	La4−O8 × 2	2.79(2)
La1−O5	2.77(1)	La2−O3	2.411(2)	La3−O9	2.726(2)		
La1−O6	2.516(2)	La2−O5	2.82(2)	La3−O10 × 2	2.93(2)		
La1−O7	2.75(1)	La2−O7	2.54(1)				
La1−O7	2.76(1)	La2−O10	2.68(1)				
La1−O8	2.52(1)	La2−O10	2.88(2)				
W1−O2 × 3	1.903(2)	W2−O3 × 3	1.935(2)	W3−O4 × 3	2.065(1)	W4−O7 × 3	1.84(1)
W1−O6 × 3	1.982(2)	W2−O5 × 3	1.920(2)	W3−O8 × 3	1.75(2)	W4−O10 × 3	2.02(2)
W5−O1 × 6	1.90(1) × 6	W6−O9	1.923(2) × 3				
		W6−O10	2.091(2) × 3				

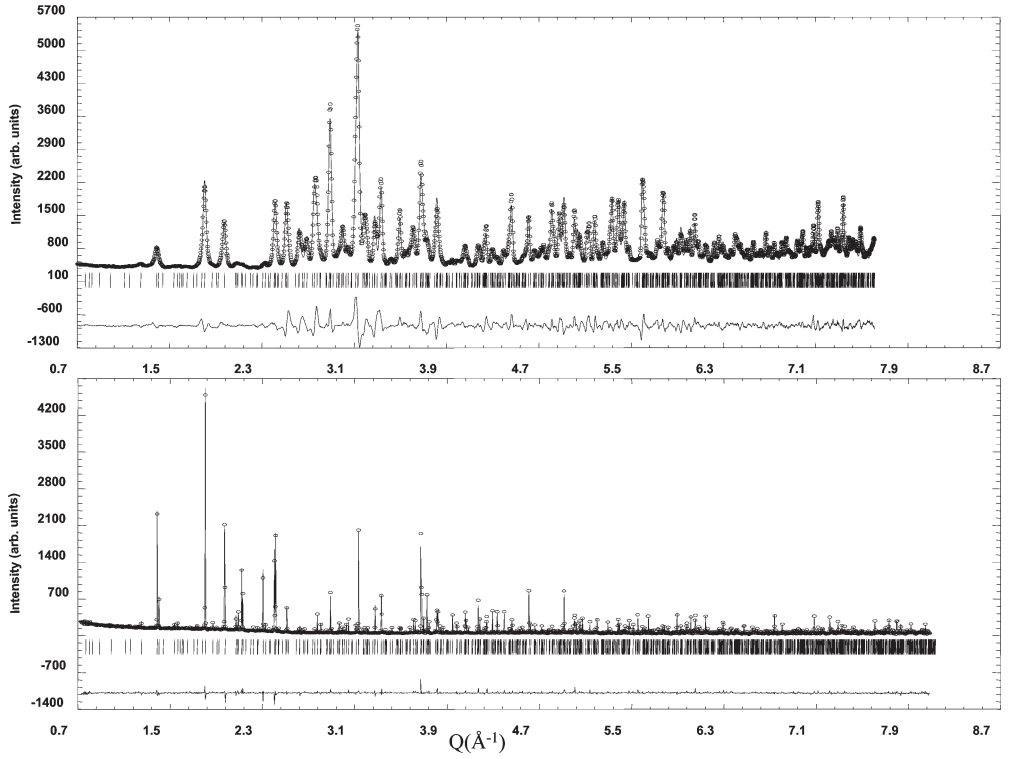

Figure 2. Diffraction patterns: (a) neutron and (b) synchrotron radiation plot, in the same q (Å^{-1}) scale. Circles represent the observed data, lines the calculated data, and ticks the peak position. The bottom shows the difference observed − calculated data.

the cell parameters of these halotungstates are similar to the $c/6$ subcell with $a = 9.4048$ Å and $c = 5.4253$ Å (S.G. $P6_3/m$), to be compared to $a = 9.0448$ Å, $c/6 = 5.447$ Å for the title compound. A comparison of the La and W atom coordinates in both compounds is provided in Table 1. The W atom in $La_3WO_6Cl_3$ is at $z = 1/4$ and 3/4, whereas the corresponding W2 in the subcell of the title compound is exclusively at $z = 1/2$ and there is an additional W1 at 0,0,0. This explains why early attempts to solve the $La_{18}W_{10}O_{57}$ structure by building a model from the $La_3WO_6Cl_3$ structure failed.

Tests in order to see if reducing the symmetry would allow the half-occupied W site to become fully ordered were made in $P31c$ and in various subgroups of $P\bar{6}2c$ and $P31c$ (*Ama*2, *Cc*) with no convincing result: the number of atomic coordinates to be refined becomes prohibitive.

Refinement and Structure Analysis. In order to stabilize the refinement, a mixed refinement has been performed from synchrotron and neutron diffraction patterns. The details of the Rietveld refinements, the atomic coordinates, and the interatomic distances are gathered respectively in Tables 2 and 3. The W4 atom, which has half the W6 as a neighbor, is the only tungsten atom presenting a high thermal parameter. Such a high thermal parameter could be interpreted as local disorder, and it should be better labeled as ADP (atomic displacement parameter). The O8 atom presents also a high thermal parameter, which could be explained with the unusual triangular coordination OM_3 (M = La1, La4, and W3) in comparison with other OM_4 tetrahedra. The low-quality fit of the neutron data (Figure 2a), in spite of the medium resolution, may be due to inhomogeneities in the sample and a strong polytypism effect (see later). Anyway, the current description of that structure, having resisted, up to now, characterization attempts, is the best we can do with these data and samples. Figure 2a and 2b presents our final Rietveld refinements, in agreement with the atomic parameters provided in Table 2.

Table 4. Calculated Bond Valence for $La_{18}W_{10}O_{57}$[a]

atom	coordination	BV sum (σ)	atom	coordination	BV sum (σ)
La1	9	3.10(5)	O1	4	2.22(6)
La2	9	3.20(5)	O2	4	2.11(6)
La3	10	2.93(5)	O3	4	2.22(6)
La4	8	3.01(5)	O4	4	2.08(5)
W1	6	5.6(1)	O5	4	2.06(6)
W2	6	5.9(1)	O6	4	2.03(5)
W3	6	6.8(1)	O7	4	2.01(3)
W4	6	5.9(1)	O8	3	2.15(8)
W5	6	6.2(1)	O9	5	1.48(5)
W6	6	4.8(1)	O10	4.5	1.6(5)

[a] $B = 0.37$ Å, $R_o(La^{3+}-O^{2-}) = 2.172$ Å and $R_o(W^{6+}-O^{2-}) = 1.917$ Å.

Bond valence calculations were performed directly by the program Bond Str[11] with the atomic position deduced from the neutron refinement, using the Brown−Altermatt empirical expression: Valence $= \sum \exp(R_o - d)/B$ with $B = 0.37$ Å.[17] The values used by the Fullprof program were for $La^{3+}-O^{2-}$ $R_o = 2.172$ Å and for $W^{6+}-O^{2-}$ $R_o = 1.917$ Å, as mentioned in ref 18. The results of the bond valence calculations for each atom type give values around the expected +3, +6, and −2 (see Table 4) for lanthanum, tungsten, and oxygen, respectively. The discrepancies between calculated and theoretical values are similar to those found in our previous structural analysis in the same phase diagram. We can mention the small values obtained for O9 and O10 even with a larger coordination number, respectively 5 and 4.5. These last two oxygen atoms are bonded to W6 and have a statistical occupancy that could introduce local distortion. These small values are also due to long oxygen−cation distances, $d(O9-La2) = 3.05(1)$ Å. Three tungsten atoms adopt an unusual trigonal prismatic coordination. These three tungsten atoms respectively, W1, W2, and W5, present very similar features: W−O distances 1.87 and 2.02 Å for W1 with an average of 1.95 Å, 1.93 Å for W2, and 1.914 Å for W5. These distances have to be compared with the W−O distances found in $Pr_3WO_6Cl_3$ and $La_3WO_6Cl_3$, respectively: 1.927 and 1.912 Å. From our knowledge, this is only the second time that such trigonal prismatic coordination is observed for tungsten atoms (Figure 3a). We believe that such trigonal prismatic coordination has never been observed in molybdates.

The second interesting structural feature is the face-shared octahedra observed between W4 and W6 atoms. An octahedral environment is rather common in many tungstates. For example, in the $BaO-WO_3$[19] system nearly all the phases adopt such a polyhedron. This is true for Ba_3WO_6,[20] Ba_2WO_5,[21] and also $Ba_3W_2O_9$.[22] The exception is $BaWO_4$, which adopts the common Scheelite structure with a tetrahedral environment.

In the last phase equilibrium diagram we observe isolated octahedra in Ba_3WO_6 and shared vertices in Ba_2WO_5. Face-shared octahedra are only observed in $Ba_3W_2O_9$ and also in $Ba_3Fe_2WO_9$.[23] In order to increase metal−metal distances, tungsten atoms move from the ideal center of the octahedra (Figure 3b). In $La_{18}W_{10}O_{57}$ the situation is even more complex: four octahedra are connected by faces, namely, W4−W6−W6−W4 (Figure 3c). The last comment is then spurious, hopefully the W6 atomic position is half-occupied, leading to the two possible sequences W4−W6−□−W4 or W4−□−W6−W4. For the crystallography, it is clear that depending on the presence or absence of W6, the W4 position will be modified along z. Accordingly, the very short W4−W6 interatomic distance 2.68 Å should be considered cautiously, and it should be compared with the W−W distance (2.94 Å) observed in $Ba_3W_2O_9$. In $Ba_3Fe_2WO_9$ the face-shared octahedra between the mixed site $(Fe^{III}/W)-(Fe^{III}/W)$ leads to 2.77 Å. The ionic radii $(W^{VI})_6 = 0.60$ Å and $(Fe^{III})_6 = 0.55/0.645$ Å (LS/HS)[24] are comparable, but electronic repulsion between two W^{VI} should be higher. The minimum W−W distance is observed in Bi_2WO_6[25] at 2.70 Å, but in this case the octahedra shared vertices. Such a situation could partially explain the longer bond distances between W6−O9 and W6−O10 and also the strong thermal agitation observed for W4.

Thanks to $La_3WO_6Cl_3$ (Figure 4a) and $Ba_3W_2O_9$ (Figure 4b) structural information, a $La_{18}W_{10}O_{57}$ structural analysis can be undertaken. A study in the (a,b) plane (see Figure 4c) reveals that it was a mixture of the two structures $La_3WO_6Cl_3$ and $Ba_3W_2O_9$. Like $La_3WO_6Cl_3$, our structure presents a $[WO_6]^{6-}$ trigonal prism surrounded by three lanthanum. Concerning the WO_6

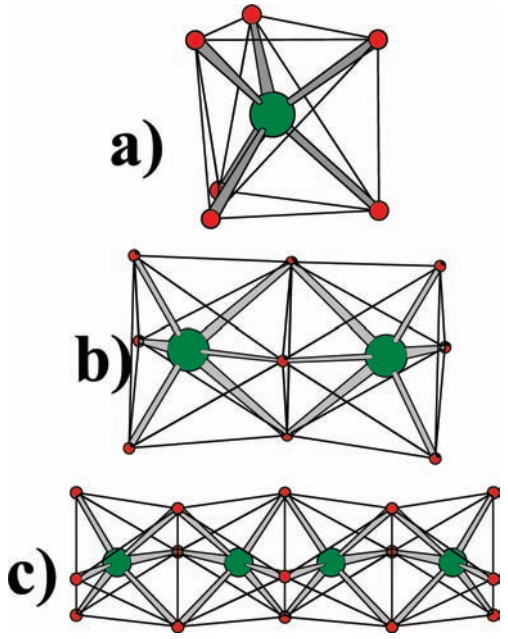

Figure 3. (a) Trigonal prismatic coordination of W1 observed in $La_{18}W_{10}O_{57}$, (b) W_2O_9 formed by a face-shared polyhedra observed in $Ba_3W_2O_9$, (c) face-shared polyhedra W6−W4−W4−W6 chain observed in $La_{18}W_{10}O_{57}$.

(17) Brown, I. D.; Altermatt, D. *Acta Crystallogr.* **1985**, *B 41*, 244.
(18) Brese, N. E.; O'Keeffe, M. *Acta Crystallogr.* **1991**, *B 47*, 192.
(19) Kreidler, E. R. *J. Am. Ceram. Soc.* **1972**, *55*(10), 514–519.
(20) Steward, E. G.; Rooksby, H. P. *Acta Crystallogr.* **1951**, *4*, 503–507.
(21) Kovba, L. M.; Lykova, L. N.; Balashov, V. L.; Kharlanov, A. L. *Koord. Khim.* **1985**, *11*(10), 1426–1429.
(22) Poeppelmeier, K. R.; Jacobson, A. J.; Longo, J. M. *Mat. Res. Bul.* **1980**, *15*, 339–345.
(23) Seveque, F.; Delamoye, P.; Poix, P.; Michel, A. *C. R. Acad. Sci. Ser. C* **1969**, *269*, 1536–1538.
(24) Shannon, R. D. *Acta Crystallogr.* **1976**, *A32*, 751–767.
(25) Rae, A. D.; Thompson, J. G.; Withers, R. L. *Acta Crystallogr. B* **1991**, *47*, 870–881.

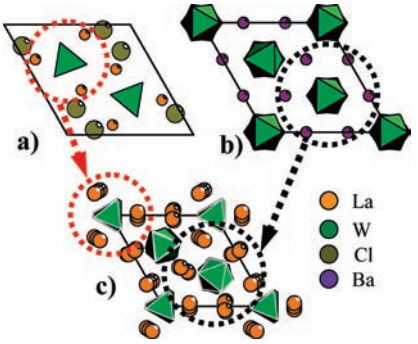

Figure 4. Units cell projection along c of (a) $La_3WO_6Cl_3$, (b) $Ba_3W_2O_9$, and (c) $La_{18}W_{10}O_{57}$. Circles indicate common structural features in the different compounds.

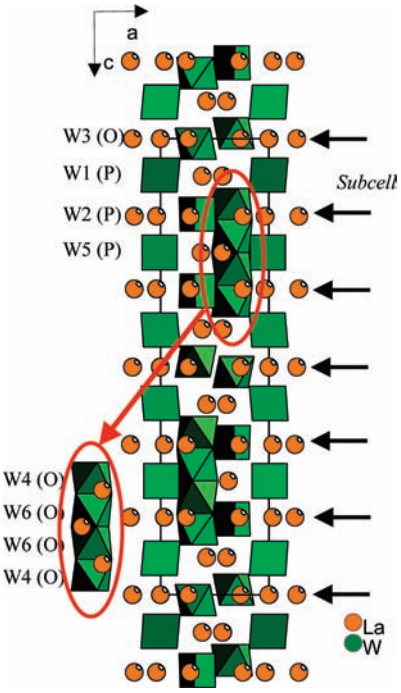

Figure 5. Unit cell projection in the (a,c) plane of $La_{18}W_{10}O_{57}$. The different tungsten coordinations are labeled: O for octahedral coordination and P for prismatic coordination. The subcell $c/6$ is marked.

octahedron, it is surrounded by six lanthanum, like in $Ba_3W_2O_9$. This mixed structure could be structurally treated as a composite structure of the two previous compounds with the formalism of superspace $(3+1)D$, which could well decrease the number of refined parameters.

The projection of the structure in the (a,c) plane reveals the stacking of the six subcells. We can also observe the different polyhedra adopted by the tungsten atoms (see Figure 5).

Polytypism. According to a previous study by Yano vskii et al.[26] from single crystal data, although the structural determination was not completed because it was not possible to obtain good crystals, the most common six-layered polytype belongs to the space group $P6_3/mmc$ (no piezoeffect detected) with cell parameters $a = 9.04(1)$ Å

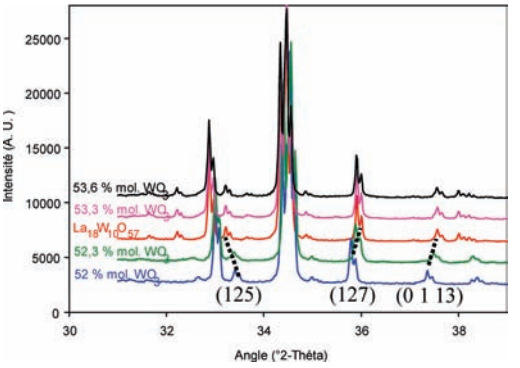

Figure 6. Powder diffraction patterns from the series (52 to 53.6 WO_3 mol %). From 52 to the nominal composition, namely, $La_{18}W_{10}O_{57}$, strong displacements of different peaks are observed. These displacements are marked with dashed lines. From the nominal composition to 53.6 no displacement is observed.

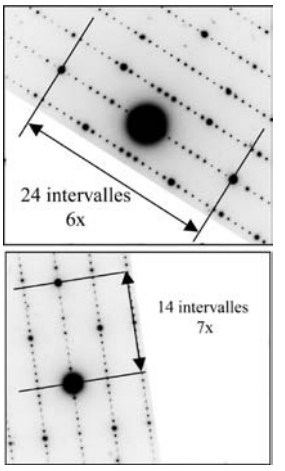

Figure 7. (a) Electron diffraction pattern of the nominal composition $La_{18}W_{10}O_{57}$ presenting c^*. Between two strong E.D. spots corresponding respectively to (002) and (00−2) 24 intervals are observed leading to 6× polytype. (b) Electron diffraction pattern of the 52 WO_3 mol % presenting c^*. Between two strong E.D. spots corresponding respectively to (002) and (000) 14 intervals are observed leading to 7×polytype.

and $c = 32.60-33.65$ Å depending on the composition of the crystal. Different polytypes of "La_2WO_6"[27] on single crystals were presented (namely, 4H $c = 22.01$ Å, 5H $c = 27.25$ Å, 6H $c = 32.64$ Å, 7H $c = 38.40$ Å, etc.). We aimed to understand and reproduce this phenomenon while varying the WO_3 molar percent between 52% and 53.6% by small steps in the synthesis of the 0.33% compound. In Figure 6, from 52% to 52.6%, we observed a rapid displacement of different peaks, namely, (1 2 5), (1 2 7), and (0 1 13) at higher or lower 2 theta positions. From 52.6% to 53.6% no displacement was evidenced. Contrary to the precedent ED study (Figure 1a), analysis for the 52% compound revealed a probable 7× superstructure (Figure 7); attempts to solve the structure from conventional X-ray data were unsuccessful. So it could be that between 50 and 52.6 WO_3 % several polytypes coexist.

Impedance and Thermal Expansion Measurements. The $La_2O_3-MoO_3$ and $La_2O_3-WO_3$ phase diagrams contain

(26) Yanovskii, V. K.; Voronkova, V. I. *Sov. Phys. Crystallogr.* **1975**, *20*, 354–355.

(27) Yanovskii, V. K.; Voronkova, V. I. *Sov. Phys. Crystallogr.* **1981**, *26* (3).

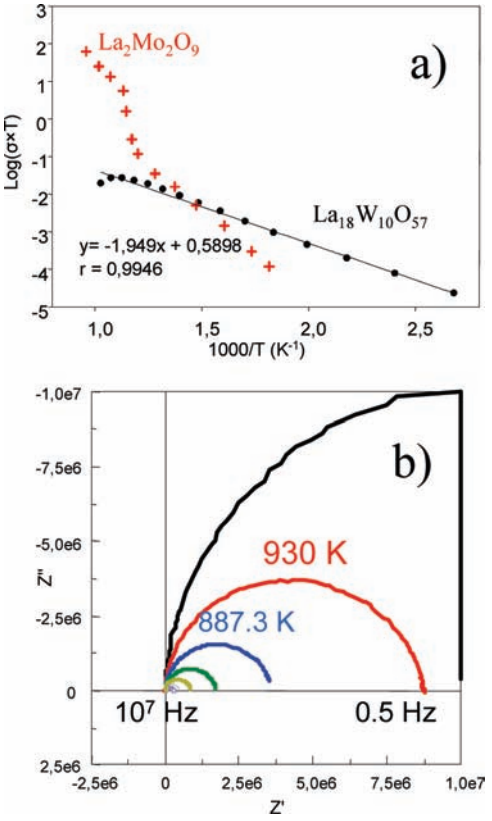

Figure 8. (a) Arrhenius plot of $La_{18}W_{10}O_{57}$ and $La_2Mo_2O_9$. (b) ac impedance plot of $La_{18}W_{10}O_{57}$ at various temperatures.

a number of compounds with interesting ionic conduction and thermal expansion properties, for example the fast ion conductors $La_2Mo_2O_9$[1] and $Y_2Mo_3O_{12}$ [28] for the thermal expansion behavior. Accordingly we have investigated these two properties in $La_{18}W_{10}O_{57}$. The same properties were also studied by Kovalevsky[29] in $La_2W_{1.25}O_{6.75}$.

The thermal expansion coefficient was measured by high-temperature X-ray diffraction. We found $\alpha_{30,1000} = 14.4\ 10^{-6}\ K^{-1}$, which is comparable with the result obtained by Kovalevsky with a dilatometric experiment, $\alpha = (10.9 \pm 0.3) \times 10^{-6}\ K^{-1}$. This value is slightly larger than the one obtained from La_2WO_6, $\alpha_{30,1000} = 11.6 \times 10^{-6}\ K^{-1}$.

The total conductivity of the sample has been obtained from an equivalent electrical circuit and a fit with Zview.[30] The Arrhenius plot of the $La_{18}W_{10}O_{57}$ conductivity is shown in Figure 8a. It is close to be linear, and we have deduced E_a after a linear regression, which is close to 0.39 eV, corresponding to 103 kcal/mol, which is comparable to 105 kcal/mol found by Kovalevsky in $La_2W_{1.25}O_{6.75}$. These authors have also underlined by efficiency Faradic study that $La_2W_{1.25}O_{6.75}$ is a mixed conductor. However, electronic conductivity prevails under an atmospheric environment; at 1170 K, the conductivity is $1.3 \times 10^{-4}\ S \cdot cm^{-1}$. We also notice that in the ac impedance plot no Warburg behavior is observed for the low frequencies. Such Warburg behavior is observed as a straight line corresponding to the usual pure ionic conductors (Figure 8b). By comparison, we find, after extrapolation of our results, a conductivity of $9.0 \times 10^{-5}\ S \cdot cm^{-1}$. Figure 8a shows the comparison between $La_{18}W_{10}O_{57}$ and $La_2Mo_2O_9$ in terms of conductivity. Our compound does not undergo a conductivity jump, and its increase with temperature is less notable. In the low-temperature region, the total conductivity is slightly higher than $La_2Mo_2O_9$; this is mainly due to the electronic part of the total conductivity of $La_{18}W_{10}O_{57}$.

Conclusion

The present study deals with $La_{18}W_{10}O_{57}$ *ab initio* structural determination from powder diffraction. The structure exhibits original tungsten coordinations that could be described as a mixing between two particular structures: $La_3WO_6Cl_3$ for trigonal prisms and $Ba_3W_2O_9$ for face-sharing octahedra. The structure shows a subcell $c' = c/6 = 5.45$ Å, and it should be present as the 6H polytype. Another polytype has been observed: 7H. Thermal expansion is on the same order of La_2WO_6. Ionic conductivity results are in good agreement with preceding studies. Ionic conductivity properties are not as notable as the $La_2Mo_2O_9$ case, but $La_{18}W_{10}O_{57}$ presents interest.

Acknowledgment. We would like to thank the ESRF council, who accepted our proposal and permitted us to access BM01 (Grenoble, France). The authors are grateful to Van Beek Wouter, their local contact at Synchrotron, for his technical assistance on the beamline.

(28) Gates, S. D.; Lind, C. *J. Solid State Chem.* **2007**, *180*(12), 3510–3514.
(29) Kovalevsky, A. V.; Kharton, V. V.; Naumovich, E. N. *Mater. Lett.* **1999**, *38*, 300–304.
(30) Johnson, D. *Z-view version 2.9b*; Scribner Associates Inc., 2004.